Journal of Marine Science and Technology manuscript No.
(will be inserted by the editor)

A crack propagation simulation for a steel CHS T-joint employing an advanced shell-solid finite element modeling

S. Tanaka · K. Maeda · H. Takahashi · H. Okada · K. Yagi · N. Osawa

Received: date / Accepted: date

Abstract An efficient crack propagation (CP) simulation system based on a shell-solid finite element (FE) modeling is newly established. Three-dimensional (3D) CP simulation for a curvilinearly propagating surface crack in a steel circular hollow section (CHS) T-joint is carried out. Entire model is generated by a shell FEs, and cracked welded part is generated by a solid FEs. They are connected with a rigid body element (RBE). Stress intensity factors (SIFs) are computed for analyzing CP rate and CP direction of the crack employing virtual crack closure-integral method (VCCM) with quadratic tetrahedral FEs. When the crack extends, only solid model is regenerated. To examine effectiveness of the modeling, fatigue testing and simplified CP simulation results are employed. Hot spot stress (HSS) and weld toe magnification factor (Mk factor) formulas are used for the simplified CP method. CP phenomena of the fatigue test are studied through the fatigue assessment methods.

S. Tanaka, K. Maeda, H. Takahashi
Graduate School of Advanced Science and Engineering, Hiroshima University, 4-1, Kagamiyama 1-chome, Higashi-Hiroshima, 739-8527, Japan
E-mail: satoyuki@hiroshima-u.ac.jp

H. Okada
Department of Mechanical Engineering, Faculty of Science and Technology,
Tokyo University of Science, Japan

K. Yagi
Shin Kurushima Sanoyas Shipbuilding Co,.Ltd., Japan

N. Osawa
Department of Naval Architecture and Ocean engineering, Osaka University, Japan

Keywords Fracture Mechanics Analysis · Tubular Joint · Shell-Solid Modeling · Weld Toe Magnification Factor

1 Introduction

Steel tubular joints have been adopted in several offshore, civil and architectural structures as a consequence of excellent structural and mechanical properties such as high strength-to-weight ratio, non-directional buckling and flexural strength capacity. Some typical CHS joints are Y-, K- and X-joints. They are commonly employed in jackets and offshore platforms [1]. The joints are composed of steel CHS members and are connected by welding each other. Complicated stress distribution is induced at the brace and chord intersections due to the complex fabricated geometry, 3D curved-shaped weld toe and its residual stress. Such kinds of characteristics lead the convoluted fatigue and fracture phenomena. Additionally, welded structures are very large, not only local behaviors but also global response should be studied in the fatigue strength evaluation.

Several fatigue strength assessment methodologies such as nominal stress approach [2,3], HSS approach [4,5] and CP approach [6-14] have been developed and extensively adopted for ships and offshore structures. They are summarized in [15,16]. Fatigue design recommendations of these offshore steel structures are established in design rules and regulations, *e.g.*, UK Den [17] and DNV-RP-C203 [18]. Furthermore, a number of research works have been performed. Bowness and Lee [19,20] proposed SIF solutions of weld toe cracks in offshore tubular joints. Qian *et al.* [21-24] analyzed mode mixity of a surface crack in X- and K-joints. Wang and Lambert [25] and Qiang and Wang [26] analyzed the

SIFs of welded joints by weight function methods. Ahmadi *et al.* [27-30] solved stress concentration factors (SCFs) for several tubular joints and proposed the simplified formulas. Gadallah *et al.* [31] investigated mixed-mode SIFs in tubular T-joint taking welding residual stress into account. Maeda *et al.* [32] examined a curved fracture surface generated in a T-shaped tubular joint employing extended FE method.

3D CP simulation of a T-joint was carried out using a full solid FE model in the previous study of the authors [33]. Remeshing is required for the entire FE model in each sequentially crack extension procedure. Although half FE model is employed by means of symmetrical boundary condition (BC) on the corresponded plane, the computational cost is still expensive not only for the remeshing process but also for the solution procedures. In addition, symmetrical BC cannot provide the satisfactory results when the cracks are large compared to the whole joint. Yagi *et al.* [34] evaluated the fatigue life of T-shaped tubular joints for weld toe curvature radii ρ=3, 6 and 11 mm. The fatigue life cycles were assessed employing S-N curves, CP simulation with Mk factor formulas, and CP simulation with full solid FE models. Results with the formulas were also examined employing different HSS evaluation techniques.

In the present study, a new fatigue testing result for ρ=16 mm joint is presented. A shell-solid CP simulation system is then proposed to investigate the CP behaviors of the ρ=16 mm joint. The system is operated based on FEM (Finite Element Method) pre-process software (pre-software) TSV-Pre on Windows system [35]. The whole joint structure is modeled by triangular/quadrilateral shell FEs, and welded portion/cracked region/intersection of chord and brace are modeled by quadratic tetrahedral solid FEs. They are connected by a Rigid Body Element 3 (RBE3). VCCM with quadratic tetrahedral FEs [36] is employed to analyze mixed-mode SIFs which are appointed to predict the CP rate and CP direction. The SIFs calculation is carried out in TSV-Pre batch process [35]. Computation time is reduced and numerical accuracy is kept by the proposed shell-solid modeling compared with the full solid modeling. Handling of FE model is relatively easy. When the crack extends, only cracked solid model is regenerated and a new shell-solid model is established.

CP phenomena are investigated employing not only the advanced CP system but also simplified formulas. Mk factor formulas and HSS are employed in the simplified formulas CP simulation. Bowness and Lee [19,20] proposed the CP simulation technique for a cracked tubular joint. HSS is evaluated by the intact model based on UK Den [17,37]. Degree of bending (DOB) is defined to separate stresses at the weld toe into membrane and bending components. An empirical formula of a surface cracked body, *i.e.*, Raju-Newman equation [38] is adopted to evaluate mode-I SIF. CP simulation is carried out based on Paris' law. High-speed CP simulation can be obtained by employing Mk factor formulas and HSS. The relevancy of the simplified formula based CP simulation is also discussed for the tubular joint.

This paper is structured as follows. A fatigue test result of T-shaped tubular joint is presented in Section 2. Shell-solid modeling and CP simulation system are shown in Section 3. Analysis procedures for simplified CP simulation based on Mk factor formulas and HSS are described in Section 4. In Section 5, fatigue test results are examined employing the two fatigue strength assessment methods. Concluding remarks arising from this study are given in Section 6.

2 Fatigue tests for steel T-shaped tubular joints

2.1 Overview of the test specimen

Fatigue tests were performed for steel T-shaped tubular joints. Four joints were employed. Size, material and fabrication process were same but curvature radii of weld toe were different. The toe was ground and trimmed smoothly. Fatigue tests were carried out in Kawasaki Technology Co. Ltd., Japan. Fatigue testing results of the joints with ρ=3, 6 and 11 mm were discussed in [32-34]. New results of ρ=16 mm specimen are shown.

Size of the joint is drawn in Fig. 1(a). Outer diameter of chord was D=406.4 mm and the wall thickness was T=12.7 mm and the length was L=1,386 mm, while outer diameter of brace was d=139.7 mm and the wall thickness was t=5.0 mm. The brace and chord were joined by fusion welding. Welding condition is included in [34]. Overall view of the joint is taken in Fig. 1(b). Curvature radius of weld toe at north saddle is presented in Fig. 1(c). The geometry was cast by an impression material. Chemical composition and mechanical properties of the base metal are shown in Tables 1 and 2, respectively.

Geometric parameters [22] of the tubular joint were α=6.82, β=0.34, γ=16 and τ=0.39. Where α is chord length to the chord outer radius ratio ($=2L/D$); β is brace outer diameter to the chord outer diameter ratio ($=d/D$); γ is chord outer radius to the chord wall thickness ratio ($=D/2T$) and τ is brace wall to the chord wall thickness ratio ($=t/T$), respectively.

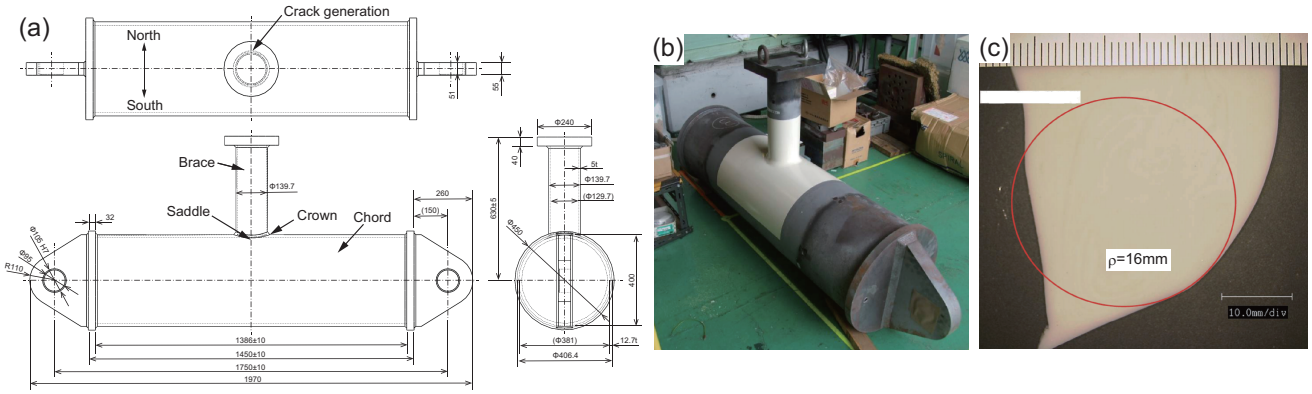

Fig. 1 T-shaped tubular joint specimen: **a** Drawing, **b** Overall view of the joint, **c** Curvature radius at north saddle cast by an impression material

Table 1 Chemical analysis of the base material

%C	%Mn	%P	%S	%Cr	%Nb	%Cu	%Mo	%Ni	%Si	%Ti	%V	%Al	%Sn	%B	CE(IIW)	CE(Pcm)
.086	0.630	.010	.003	.017	.021	.017	.002	.020	.140	.011	< .003	.033	< .002	< .0003	.19	.12

CE Carbon Equivalent; if %C >0.12 $CE(IIW) = C + Mn/6 + (Cr + M_0 + V)/5 + (Ni + Cu)/15$

CE Carbon Equivalent; if %C ≤0.12 $CE(Pcm) = C + Si/30 + (Mn + Cu + Cr)/20 + Ni/60 + M_0/15 + V/10 + 5B$

Table 2 Mechanical properties of the base material

Test Freq	Test Sample	Heat Treatment	Yield Strength (MPa)	Tensile Strength (MPa)	%Elongation	%Elongation $L_0 = 5.65\sqrt{S_0}$	Absorbed Energy (J)	Shear Area %
H	ChL	A					387	100
H&B	LT	A	410	500	34	32		

L_0-Gauge Length; S_0-Original Cross-sectional Area; H-Heat; B-Batch; A-Aged

LT-Longitudinal Tensile; ChL-Longitudinal Charpy Impact Test

Table 3 Load history and cumulative fatigue cycles

N	ΣN	$P_{\max}$ kN	R	
133,000	133,000	190	0.01	5 % drop
128,000	261,000	190	0.01	Crack penetration
36,643	297,643	190	0.01	Specimen failure

2.2 Experimental results

Two kinds of tests were carried out, *i.e.*, static loading test and cyclic loading test. In the static loading test, surface strains around north and south saddles were evaluated by strain gauge measurements. Results are compared with FE results. The detail discussion is shown in Section 5.

A sinusoidal pulsating tensile load was employed in the cyclic loading test. Maximum load $P_{\max}$ was 190 kN and load ratio was R=0.01. Load history and cumulative fatigue cycles are presented in Table 3. A surface crack was generated and then extended. A five percent drop of strain gauge amplitude was remarked around north saddle at 133,000 cycles. The crack was penetrated the chord wall at 261,000 cycles. The through crack was further propagated and the test was terminated at 297,643 cycles. CP behaviors are shown in Fig. 2(a)-(d) as well as the number of loading cycles. A small surface crack was found in Fig. 2(a). The surface crack is extended as presented in Fig. 2(b). The crack penetrates the chord wall in Fig. 2(c). The through crack develops around the weld as shown in Fig. 2(d).

Fractured specimen is presented in Fig. 3(a). A beach mark (BM) technique was applied to analyze the CP behavior. When introducing BMs, 20,000 cycles were applied at R=0.5. The crack was penetrated the chord wall, and the crack was curved along the weld toe. Fracture surface and BMs are shown in Fig. 3(b). Close-up view of the fracture surface is presented in Fig. 3(c). Total eight BMs (BM1-BM8) were observed until crack penetration. The defect was initiated 3.6 mm offset from the center line of the joint. The surface crack was propagated almost symmetrical and it was a semi-elliptical shape. The surface crack size is summarized in Table 4.

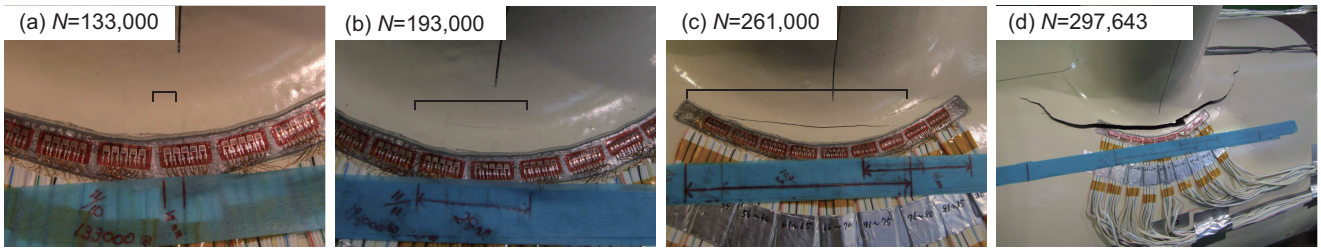

Fig. 2 CP behaviors at north saddle of the joint: **a** N=133,000, **b** N=193,000, **c** N=261,000, **d** N=297,643

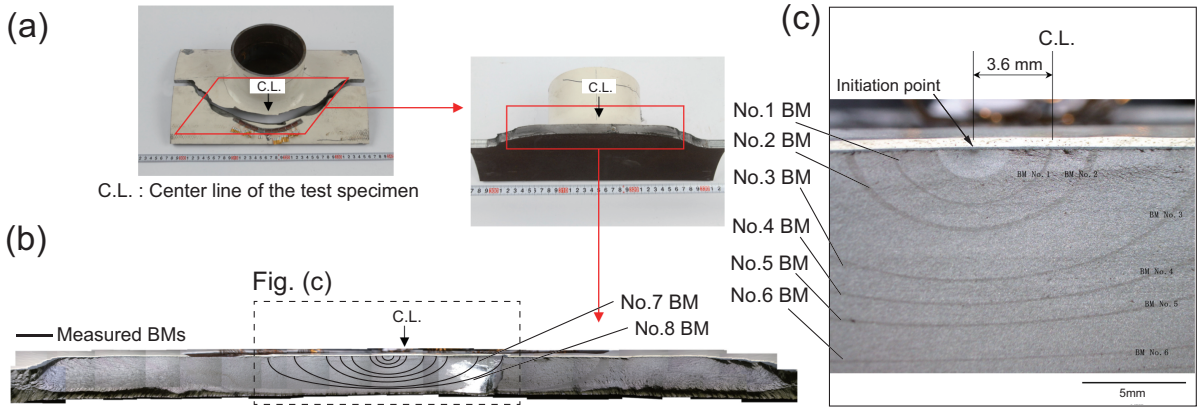

Fig. 3 BMs on the fracture surface: **a** Fractured specimen, **b** Fracture surface and BMs, **c** Close-up view of BMs

Table 4 Fatigue cycles and surface crack size for each BM No.

BM No.	cycles	2c mm	a mm
1	133,000	7.6	2.6
2	151,000	11.3	3.8
3	181,000	22.3	6.3
4	193,000	30.1	7.5
5	203,000	37.2	8.4
6	221,000	55.0	10.1
7	231,000	68.1	10.9
8	261,000	99.4	12.7

3 A shell-solid modeling of a cracked T-shaped tubular joint

Computational cost of full solid modeling is rather expensive in terms of mesh generation and solution procedures, as well as handling of the model on computers. Methodologies such as zooming method [39], global-local FEM [40-47] and shell to solid transition elements [48-51] were proposed to analyze structural mechanics problems including global and local behaviors.

An advanced CP simulation system employing shell-solid modeling is developed. The system is operated based on FEM pre-software TSV-Pre on Windows system [35]. CP simulation system using full solid modeling as well as the mixed-mode SIFs evaluation method was previously discussed [33]. In this section, a CP simulation system employing the shell-solid modeling is mainly described.

A flowchart of the CP simulation is presented in Fig. 4(a). Both the whole joint and the welded joint part including detailed weld geometry are arranged by 3D-CAD. Neutral surfaces of brace and chord are extracted. They are imported to the pre-software. FE model with triangle/quadrilateral shell elements is generated for the chord and brace models. A surface crack is located around the weld and local parameters are set for the mesh generation of solid model. Solid FE model is prepared with quadratic tetrahedral FEs for the welded potion by an automatic mesh generation system. The chord, brace and cracked welded joint part are merged. A linear elastic analysis was performed after the material properties are assigned and load and BCs are enforced. Mixed-mode SIFs are then computed employing VCCM technique [36]. CP rate and CP direction are determined based on the SIFs. Remeshing of the solid FE model is required for the new crack growth. The procedures are incremented.

Accuracy of SIFs employing VCCM method was confirmed for embedded crack and surface crack in [36]. Also, accuracy in SIFs of the CP software was confirmed for cruciform welded joints in [47] by comparing with the reference solutions using MSC.Marc [52].

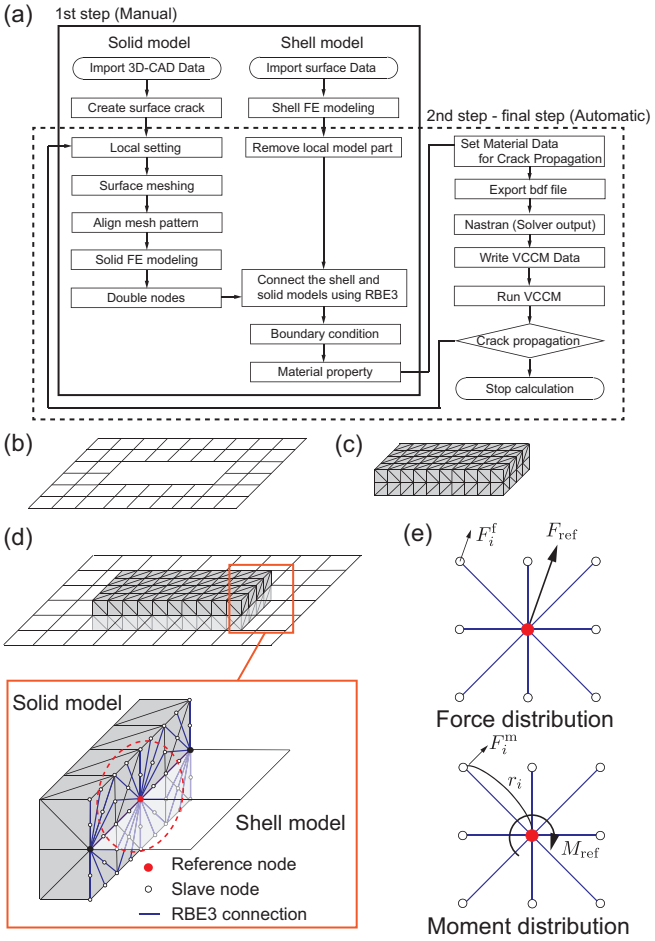

Fig. 4 Flowchart and a shell-solid modeling for CP simulation system: **a** Flowchart of the simulation, **b** A shell model, **c** A solid model, **d** A shell-solid model using RBE3s, **e** Force and moment distribution for 2D case.

A schematic diagram of shell-solid modeling is drawn in Fig. 4(b)-(d). Shell and solid models are respectively shown in Fig. 4(b) and (c). RBE3 connection is presented in Fig. 4(d). The shell model is placed at mid-plane of the solid model. Same plate thickness is assumed to generate the shell-solid model. Nodes of shell model represent the reference nodes, and nodes of solid model denote slave nodes for RBE3s, respectively. The strategy of the RBE3 connection is that the force and moment are imposed through a reference node to the slave nodes as shown in the red circle in Fig. 4(d).

A simple 2D example of the force and moment distribution of RBE3 connection from the reference node to the slave nodes are shown in Fig. 4(e). They can be written, as:

$$F_i^{\mathrm{f}} = F_{\mathrm{ref}} \frac{\omega_i}{\sum_k \omega_k}, \quad F_i^{\mathrm{m}} = \frac{M_{\mathrm{ref}} \omega_i r_i}{\sum_k \omega_k r_k^2}, \tag{1}$$

where F_{ref} and M_{ref} are force and moment of the reference node. F_i^{f} and F_i^{m} are force of i-th slave node corresponded force and moment distribution. ω_i is a weighting factor. r_i is distance between reference node and i-th slave node. As for the moment distribution in Fig. 4(e), this example is for 2D case and torsional moment is applied to the reference node. For 3D case, each reference and slave node has six degrees of freedom (DOFs). Bending moment can transfer between the shell and solid models taking configuration of the reference/slave nodes into account. For further detail, the readers are referred to the reference manual [52].

Effective 3D CP simulation can be carried out with the shell-solid modeling. Although mixed-mode SIFs of a stationary surface crack were analyzed in [47] and nonlinear buckling problem of a cracked plate was solved in [53] using the shell-solid modeling, CP simulation has not performed yet.

4 A simplified CP simulation employing *Mk* factor formulas

Mk factor [54] is defined as a ratio of mode-I SIF, *i.e.*, K value, with and without attachment of a welded joint, as:

$$Mk = \frac{K_{(\text{in plate with attachment})}}{K_{(\text{in same plate but with no attachment})}}. \tag{2}$$

The Mk factor approach has been implemented to several 2D and 3D welded joint models [55-58]. Bowness and Lee developed new Mk factor formulas of T-butt welded joint for small and large weld toe radii based on an extensive FE database [59,60]. Additionally, Mk factor formulas were employed for cracked tubular joint problems [19,20]. K value evaluation technique is briefly described.

An illustration of a surface cracked tubular joint under a remote stress σ_{nom} ($=P/A$) is shown in Fig. 5(a). P is an applied load and A is a cross-section area of the brace. Depth and half width of the surface crack are a and c, respectively. K value of the surface cracked tubular joint K_{TJ} can be evaluated as:

$$K_{\mathrm{TJ}}^i = [Mk_{\mathrm{m}}^i \, M_{\mathrm{m}}^i \, SCF(1 - DOB) + Mk_{\mathrm{b}}^i \, M_{\mathrm{b}}^i \, SCF \cdot DOB]\sigma_{\mathrm{nom}}\sqrt{\pi a}, \tag{3}$$

where Mk_{m}^i and Mk_{b}^i are Mk factor formulas for a T-butt joint in terms of membrane and bending stresses, respectively. Superscript i represents position of the crack front, *i.e.*, "i"="a" is at deepest point and "i"="c" is at crack mouth. M_{m}^i and M_{b}^i are shape factors for a cracked flat plate which are adopted in Raju-Newman equations [38]. Equations M_{m}^i and M_{b}^i are included in the report [61]. SCF ($=SCF_{\mathrm{out}}$) is a SCF at the weld toe, *i.e.*, $SCF=HSS/\sigma_{\mathrm{nom}}$. HSS means hot spot

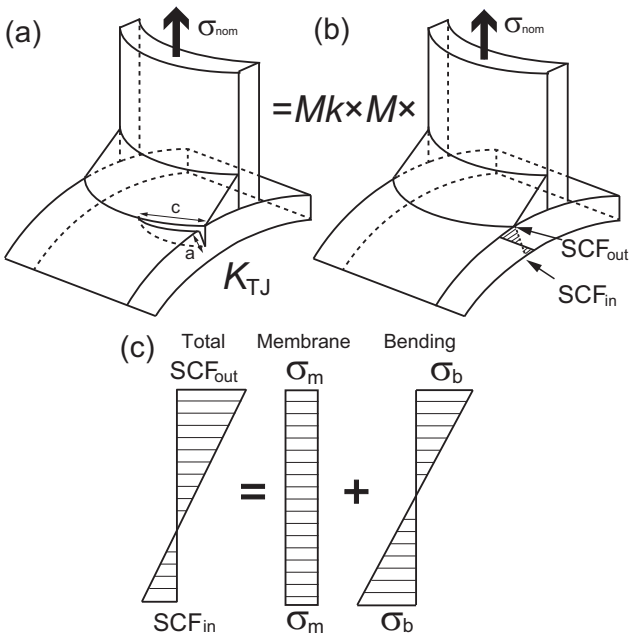

Fig. 5 A technique to evaluate K value employing Mk factor: **a** A surface cracked tubular joint, **b** K value evaluation technique using an intact tubular joint model and Mk factor, **c** Definition of SCF_{in} and SCF_{out}

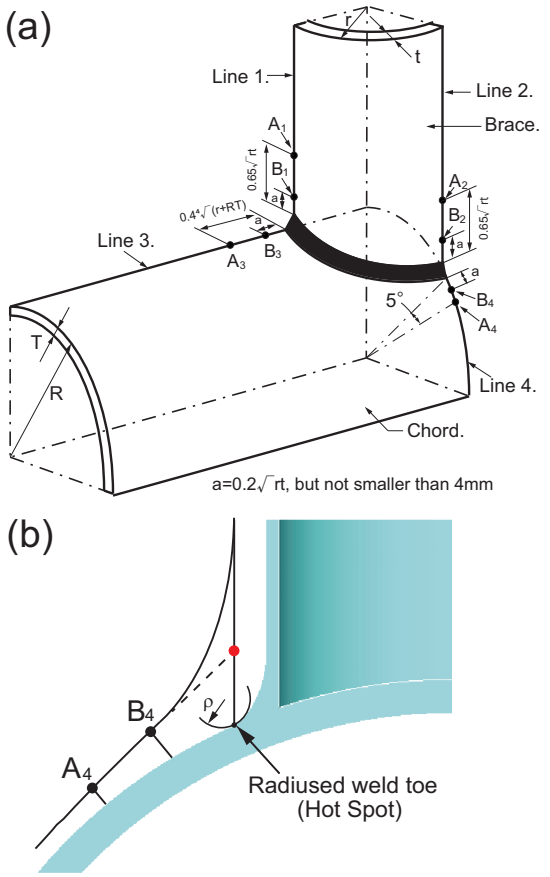

Fig. 6 HSS evaluation technique for UK Den: **a** ROPs, **b** Definition of hot spot and linearly extrapolated HSS

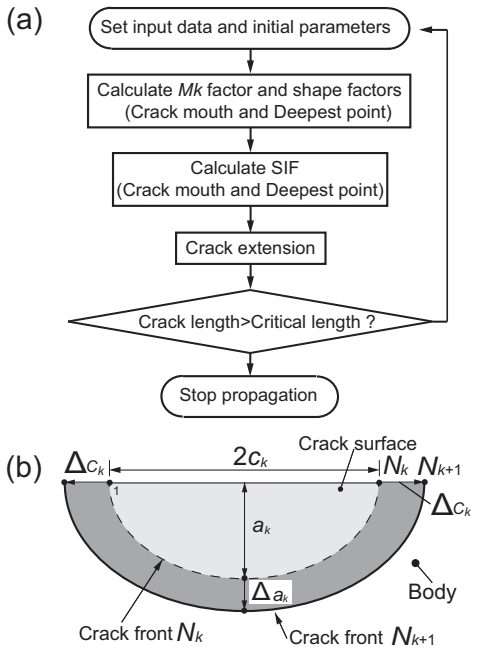

Fig. 7 Analysis procedure for a CP simulation employing Mk factor formulas

stress. DOB is defined, as:

$$DOB = \frac{\sigma_{\mathrm{b}}}{\sigma_{\mathrm{m}} + \sigma_{\mathrm{b}}} = \frac{1}{2}\left(1 - \frac{SCF_{\mathrm{in}}}{SCF_{\mathrm{out}}}\right), \tag{4}$$

where SCF_{in} ($=\sigma_{\mathrm{m}}$-σ_{b}) and SCF_{out} ($=\sigma_{\mathrm{m}}$+σ_{b}) are SCFs of inner and outer surfaces of an intact tubular joint model at the weld toe as shown in Fig. 5(b) and (c). σ_{m} and σ_{b} are stress components due to membrane and bending deformations.

Two kinds of Mk factor formulas [59] are available, *i.e.*, for small weld toe radius ($0.0 \leq \rho/T < 0.1$) and for large weld toe radius ($0.1 \leq \rho/T$) where ρ/T is a ratio of weld toe radius to the chord thickness. In the present case, the ratio is $\rho/T = 1.26$. Formula for large weld toe radius is chosen. These formulas can be obtained from the website [19].

UK Den is employed to evaluate the HSS [17,20,37]. HSS read out points (ROPs) are shown in Fig. 6(a). Linear and quadratic extrapolation techniques are adopted. A_4, B_4 and C_4 are regarded as ROPs in quadratic extrapolation. C_4 is equidistant from A_4 with reference to B_4, *i.e.*, $C_4 = 2A_4 - B_4$. The weld toe is ground and defined as "radiused weld toe" which is illustrated in Fig. 6(b). It is an intersection of chord surface and weld toe curvature. HSS is evaluated at the radiused weld toe. Hoop stress of the chord surface is employed for evaluation of ROPs. For example, a linear extrapolation technique is schematically illustrated in Fig. 6(b).

A simplified CP simulation is carried out based on Mk factor formulas. Flowchart of the simulation is shown

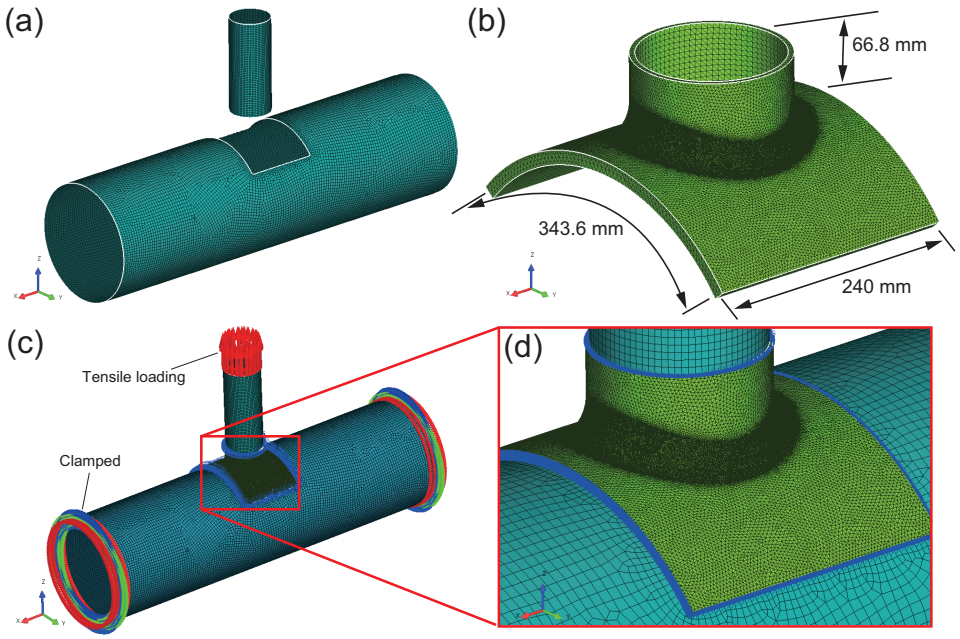

Fig. 8 A shell-solid model for an intact T-shaped tubular joint: **a** A shell model, **b** A solid model, **c** A shell-solid model, **d** Close-up view of the intersection

in Fig. 7(a). First, input data and initial parameters are arranged. A semi-elliptical surface crack is assumed as the initial crack. Mk factor formulas Mk^i_{m} and Mk^i_{b}, shape factors M^i_{m} and M^i_{b} (i=a and c) are computed. SCF and DOB are evaluated by the input data and FE results of the intact model, K^i_{TJ} is computed for mouth and deepest point of the surface crack employing Eq. (3). Crack shapes for k-th and (k+1)-th propagation steps corresponded to N_k and N_{k+1} cycles are drawn in Fig. 7(b). Paris' law is adopted and amounts of crack extension Δa_k and Δc_k are evaluated. New crack shape for (k+1)-th step is generated. The procedures are incremented and the crack is extended until critical length. Speedy CP simulation can be carried out employing Mk factor formulas.

5 Results and discussion

5.1 Results for the static loading test

An illustration of the shell-solid modeling is presented in Fig. 8(a)-(d). Shell and solid models are separately arranged. The shell model is shown in Fig. 8(a). Four node quadrilateral shell FEs are employed. The element size is around 5.0-10.0 mm. Shell elements are removed at the brace-chord intersection. Total nodes and elements of shell model are 23,988 and 23,684, respectively. Solid model including the detailed welding geometry is described in Fig. 8(b). The intersection of the brace and chord is modelled with the arc dimension of 343.6×240 mm and 66.8 mm height for the brace. Quadratic tetrahedral FEs are employed for entire solid model and its size is around 4.0 mm. Very fine mesh (around 0.8 mm) is used around the weld to provide the accurate stress concentration. Total nodes and elements of solid model are 678,503 and 429,531, respectively.

The shell-solid model is presented in Fig. 8(c). A close-up view of the intersection is shown in Fig. 8(d). The shell model is placed at mid-plane of the solid model. They are connected with each other using RBE3s. Tying relations are automatically constructed in the pre-software by selecting edge of the shell model and face of the solid model. Both of the chord ends are clamped as presented in Fig. 8(c). A tensile uniaxial load 70 kN is applied to the top of the brace. Young's modulus and Poisson's ratio are E=206 GPa and ν=0.3, respectively. Material properties as well as the shell thickness are assigned after BCs are set. A linear elastic analysis is carried out. MSC.NASTRAN [62] is chosen. Element types are CQUAD4 (Quadrilateral plate element), CTETRA (Four-sided solid element) and RBE3. A CTETRA element has ten nodes. A large-scale iterative solver CASI is employed.

When the shell-solid modeling is adopted, oscillation of displacement and stress values sometimes occurs around RBEs, and it affects accuracy of the numerical results [47]. First, results of the shell-solid model are compared with those of the full solid model. A cross-section of north saddle is shown in Fig. 9(a). The weld

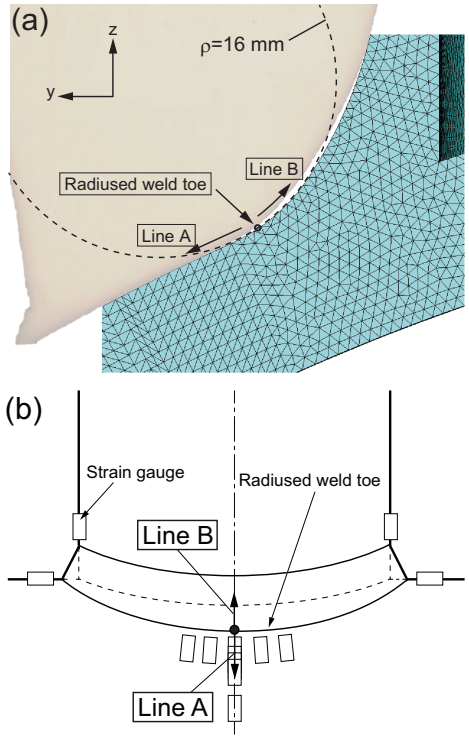

Fig. 9 Surface stress evaluation at saddle: **a** Cross-section of the FE model, **b** Strain gauge position

toe geometry is modeled by a 3D-CAD based on measurement data presented in Fig. 1(c).

Surface stress of the saddle is evaluated along Lines A and B from the radiused weld toe. Location of strain gauges are shown in Fig. 9(b). A full solid model with very fine mesh is analyzed for comparison purpose. Maximum principal stress of the chord surface are presented in Fig. 10. Stress distribution of the shell-solid model is in good agreement with that of the full solid model. It is confirmed that accurate computation can be carried out employing the solid model size.

Numerical results are compared with the experimental results. Normal stress of the chord surface at north saddle in their tangential direction are presented. For reference, measurement data at south saddle is also included. Surface stress in the experiment are evaluated by multiplying the strain measurement data and Young's modulus. The results are also shown in Fig. 10. A slightly different results are found due to the difficulty of strain gauge setting on the curved surface. However, reasonable results can be obtained.

As shown in Fig. 10, peak stress can be seen around 3.5 mm offset from the radiused weld toe. The weld toe is relatively large, *i.e.*, ρ=16 mm, and then, the peak point is shifted from the radiused weld toe. It is known that an initial crack is inclined to generate around high stress region, then, crack initiation position may also shift from the radiused weld toe. However, in the present study, initial crack is inserted at radiused weld toe to compare with the simplified CP simulation results. Hot spot is defined at the radiused weld toe in the simplified method as shown in Fig. 6(b).

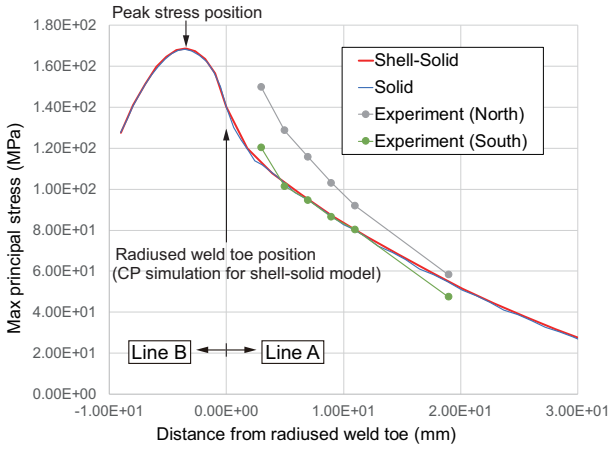

Fig. 10 Max principal stress distribution on the chord surface

5.2 Setting for the CP simulations

5.2.1 A cracked shell-solid model

CP simulation is carried out. Shell-solid FE model with an initial crack is shown in Fig. 11(a). Similar to the static loading test model, 5.0-10.0 mm shell elements are employed. Number of nodes and elements of the shell model are 69,979 and 69,547, respectively. A close-up view of the solid model is presented in Fig. 11(b). The solid model size is same with the static loading case. The CP simulation system does not allow to introduce a curved crack into the FE model. A planar small semi-circular surface crack (a=0.2 mm, $2c$=0.4 mm) is assumed and it is extended to generate smooth curved crack surface. Fatigue cycles are compared when the crack size becomes almost similar with BM No.1 in Table 4. The whole solid model is divided around 5.0 mm quadratic tetrahedral FEs. The cracked part region is divided around 0.2 mm FEs. Element size along the crack front is 0.003 mm. Total number of nodes and elements of the solid model are 683,689 and 449,995, respectively.

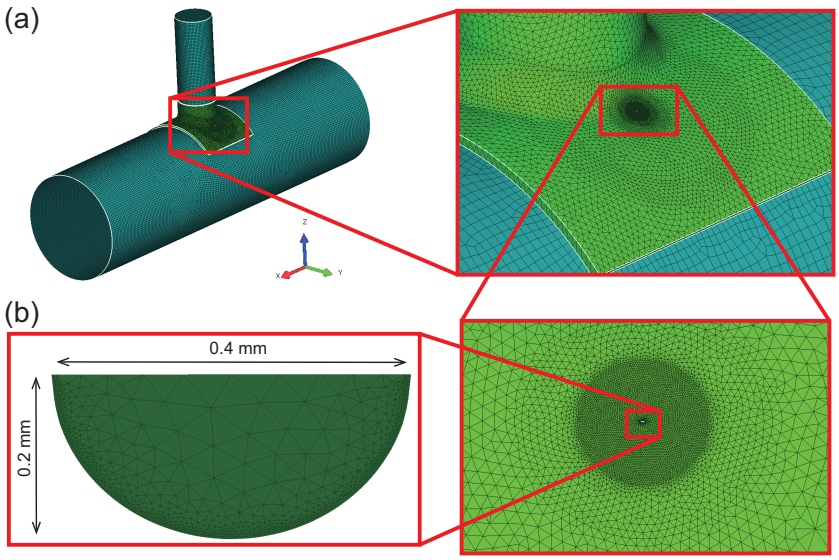

Fig. 11 A surface cracked shell-solid model: **a** Whole view, **b** Around cracked part

5.2.2 Fracture criteria for CP simulation

For CP simulation, modified Paris' law is chosen. It is given as:

$$\frac{da}{dN} = C(\Delta K_{\rm eq}^m - \Delta K_{\rm th}^m), \tag{5}$$

where C and m is material parameters, da/dN is the CP rate. The coefficients were C=2.66704e-11, m=2.75 (unit: m/cycle) and the threshold SIF $\Delta K_{\rm th}$=1.99223 (unit: MPa$\sqrt{\rm m}$) [63]. $\Delta K_{\rm th}$ is a threshold SIF, $\Delta K_{\rm eq}$ is equivalent SIF range considering mixed-mode state. It is written, as:

$$\Delta K_{\rm eq}^2 = (\Delta K_{\rm I} + B|\Delta K_{\rm III}|)^2 + 2\Delta K_{\rm II}^2, \tag{6}$$

where B is a coefficient. B=1.0 is chosen [64].

A maximum tangential stress criterion [65] is employed to predict crack growth direction. It is written as:

$$\theta = 2\tan^{-1}\left[\frac{-2\Delta K_{\rm II}}{\Delta K_{\rm Ieq} + \sqrt{(\Delta K_{\rm Ieq})^2 + 8(\Delta K_{\rm II})^2}}\right]. \tag{7}$$

$\Delta K_{\rm Ieq}$ ($=\Delta K_{\rm I}+B|\Delta K_{\rm III}|$) is amplitude of an equivalent SIF including mode-III effect.

It is noted that welding residual stress is not considered in the FE model. Material parameters and fixed BCs are same with the static loading case. A cyclic load ΔP=188.1 kN is considered and stress ratio R=0.01. Analyses are carried out until crack penetrates the chord wall.

5.2.3 CP simulation with Mk factor formulas

HSSs are examined to perform a simplified CP simulation. Outer and inner HSSs are evaluated by hoop stresses of the chord surfaces. Linear and quadratic extrapolation techniques are employed based on UK Den. A quarter solid model is used. Hoop stresses for the outer and inner chord surfaces are presented in Fig. 12(a) and (b), respectively. ROPs of A_4, B_4 and C_4 ($=2A_4$-B_4) are also included. Additionally, hoop stress of outer chord surface is also evaluated to investigate accuracy of the shell-solid model. The verification of hoop stress is shown in Fig. 12(c). Results with intact shell-solid model and with full solid model are presented. Also, edge position of the shell-solid model is drawn. Hoop stresses are different from the full solid model results around the connection. However, differences are vanished as long as the weld toe is approaching. Results with the shell-solid model and full solid model are in good agreement. Then, effectiveness of the shell-solid modeling and solid model size are confirmed.

Based on the stress evaluations, $SCF_{\rm in}$, $SCF_{\rm out}$ and DOB are given in Table 5. Similar values can be obtained for linear and quadratic extrapolation techniques. It is slightly conservative for quadratic case. Values with the quadratic extrapolation are employed for the CP simulation.

Table 5 $SCF_{\rm out}$, $SCF_{\rm in}$ and DOB

	$SCF_{\rm out}$	$SCF_{\rm in}$	DOB
UK DEn Linear	3.68	-2.34	0.817
UK DEn Quadratic	3.76	-2.42	0.821

CP simulation is carried out based on modified Paris' law in Eq. (5). Initial crack size is same with the one which is adopted in the FE computation. Mode-I SIF

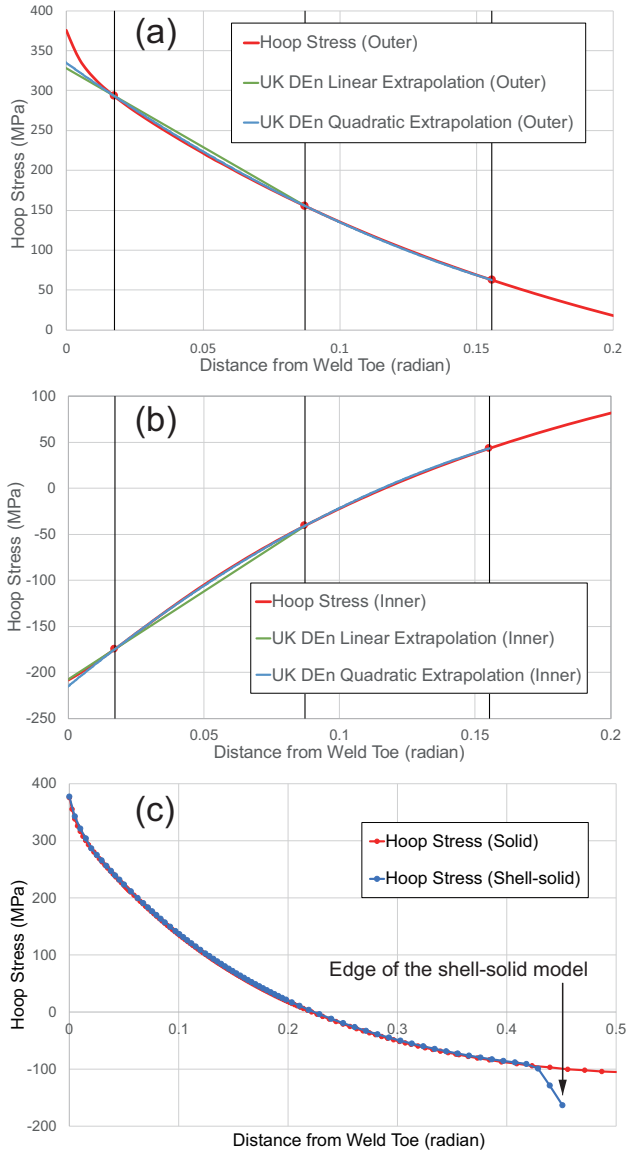

Fig. 12 HSSs evaluation for an intact tubular joint model: **a** Hoop stress of outer chord surface, **b** Hoop stress of inner chord surface, **c** Comparison of hoop stress of outer chord surface for shell-solid model with full solid model

amplitude ΔK^i_{TJ} is selected to evaluate the CP rate. It is assumed that the hot spot, *i.e.*, crack initiation position, is defined at radiused weld toe as presented in Fig. 6(b). Additionally, the surface crack is always propagating along the radiused weld toe and along perpendicular to chord surface as shown in Fig. 5(a). Analysis is carried out until crack penetrates the chord wall.

5.3 Results for the cyclic loading test

5.3.1 Computational efficiency

A tubular joint with a surface crack size a=0.2 mm and $2c$=0.4 mm is chosen. Shell-solid model is presented in Fig. 11. A cracked full solid model is also arranged for comparison purpose. Quadratic tetrahedral FEs are employed to the whole tubular joint. Computational time of the shell-solid model is compared with that of the full solid model for first five CP steps.

Same condition is employed for the FE computation. Operation system is Windows 10 Professional, and CPU is Intel® Core™ i9-10900 Processor. Memory size is 64 GB. It is a serial computing. Information of FE models and the computational time are presented in Table 6. It includes model arrangement and FE computation time of the flowchart as shown in Fig. 4(a). Computation time is reduced in the shell-solid model CP simulation by the reason of decreasing solid elements. Additionally, only solid model part is regenerated to update the crack geometry. Therefore, the proposed FE modeling is effective for large-scale cracked structures.

5.3.2 Comparison of SIFs

Cross-section of the FE model at final state is presented in Fig. 13(a). Surface crack is curved along crack width and depth directions. It means a doubly-curved surface. Here, two coordinate systems are defined to the curved crack as shown in Fig. 13(b). One is arc length. The depth is a and width is $2c$. The other is chord length, *i.e.*, the depth is a' and width is $2c'$. For CP simulation with Mk factor formulas, it is noted that the surface crack always propagates perpendicular to chord surface at the weld toe, *i.e.*, a=a'. SIFs evaluated by FEM and Mk factor formulas are investigated.

Mode-I SIF at deepest point are shown in Fig. 14(a). Until half thickness of the chord wall around a'=6.5 mm, the SIFs are gradually increased. After that, almost same values are kept until crack penetration. Additionally, the SIF results with full solid model and shell-solid model are compared in Fig. 14(a). Almost same values are obtained. Similar to the discussion on Section 5.1, efficient computation can be carried out with keeping same accuracy by using the shell-solid model.

Mk factor in Eq. (2) cannot be defined because the denominator approaches zero at deepest point under bending condition for a/T>0.5 because of the crack closure. So, Mk factor at deepest point for bending loading $Mk^{\mathrm{a}}_{\mathrm{b}}$ in Eq. (3) is set unity for conservative evaluation in [19,59], *i.e.*, if $0.005 \leq a/T \leq 0.5$ then

Table 6 FE models and computation time for first five steps.

FE model	Shell-Solid			Full solid
Element type	CQUAD4	CTETRA	RBE3	CTETRA
Nodes	69,979	683,689	312 (Master nodes)	1,572,042
Elements	69,547	449,995	-	953,131
DOFs	2,453,661			4,607,052
time [sec]	1,730			2,824

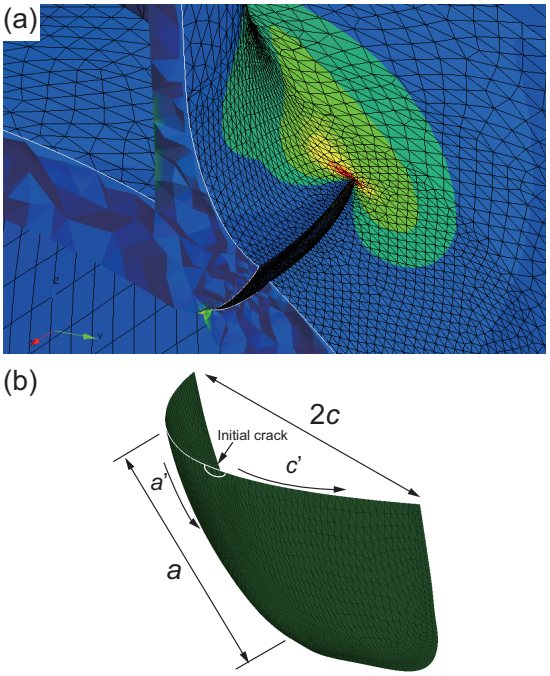

Fig. 13 CP results using the shell-solid model: **a** Cross-section of the model, **b** A doubly-curved surface

$$Mk_{\mathrm{b}}^{\mathrm{a}} = f_1 f_2, \tag{8}$$

else if $0.5 < a/T \leq 1.0$ then

$$Mk_{\mathrm{b}}^{\mathrm{a}} = 1.0, \tag{9}$$

where f_1 and f_2 are Mk factor equations. In this paper, when Eq. (8) is employed for $0.005 \leq a/T \leq 1.0$, it is called as original equation. While Eqs. (8) and (9) are employed, it is called as modified equation.

Results with Mk factor formulas at deepest point are investigated. There are two results, *i.e.*, original and modified ones in Fig. 14(a). Crack propagates until half chord wall, same values are taken. SIF employing the original equation is monotonically increased as long as the crack depth grows across the half of the chord wall thickness. When the modified Mk factor formulas are adopted, there is a jump of SIF values at the middle of the chord thickness.

Mode-I SIF at mouth are shown in Fig. 14(b). All of SIFs monotonically increases until the crack penetration. Results with Mk factor formulas give higher value than the FEM computation. Additionally, crack extensions with Mk factor formulas are larger than the FE model. Similar to the SIF results at deepest point, shell-solid and full solid modelings provide almost same SIF values for the mouth point.

Although a simplified assumption is introduced for CP simulation with Mk factor formulas, SIF results show good tendency compared with results with the 3D FE fracture modeling.

Crack path of FE model on chord surface are shown in Fig. 15. Small surface crack propagates along the weld toe. When the crack becomes large, the crack tips are apart from the weld toe. Similar tendency can be seen in the experimental results in Figs. 2 and 3. However, the crack propagates along the weld toe in the CP simulation with Mk factor formulas. Therefore, slight contradiction is occurred when the crack becomes large.

5.3.3 Comparison of aspect ratio and fatigue life

Aspect ratio and fatigue life cycles are validated among the results of shell-solid FE model, Mk factor approach and fatigue testing results. Some assumptions are introduced to carry out the simulations and to compare with the simplified formula results and therefore, precise comparison of the crack trajectories cannot be provided. However, similar tendency can be obtained.

Alternation of aspect ratio for propagated surface crack is examined. Results with the FE model and with Mk factor formulas are shown in Fig. 16. Experimental results are also presented. Coordinates a' and c' are taken for the CP simulations, while a and c are taken in the experiment. Aspect ratio is unity as the initial crack is assumed as a semi-elliptical surface crack. The ratio is gradually decreased in all cases. In Mk factor formula, it is assumed that the crack always propagates along the radiused weld toe. Since crack extension at mouth is larger than the FEM, reducing rate of the aspect ratio is faster than the FEM. The FE result agrees well with the experimental results.

Fatigue life cycles are assessed. Results are shown in Fig. 17. Since crack generation cannot be simulated in fracture mechanics approach, only fatigue life for CP

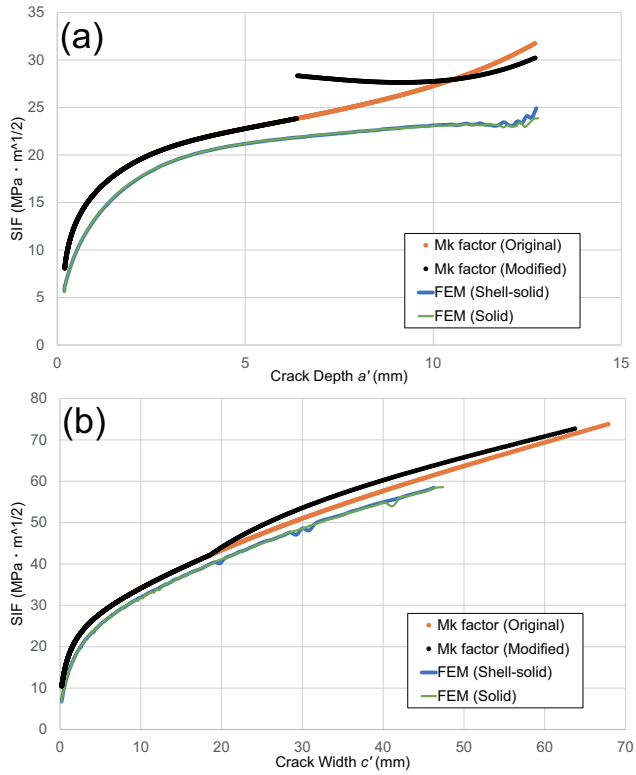

Fig. 14 Variations in mode-I SIFs: **a** Crack depth, **b** Crack width

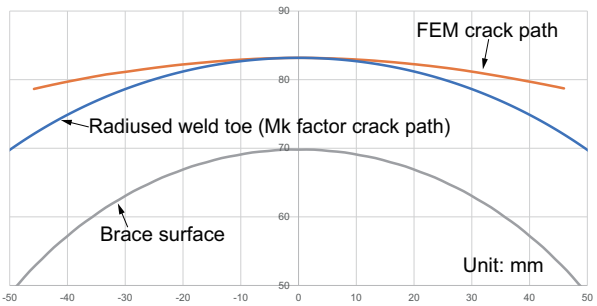

Fig. 15 Crack paths for the FEM and Mk factor approach

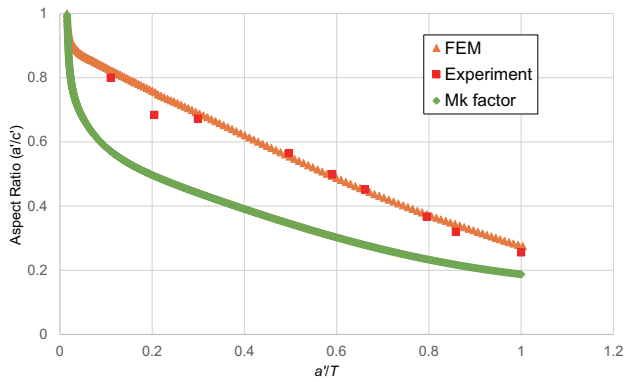

Fig. 16 Change of aspect ratio for CP simulation and experimental results

is evaluated. Based on BM No.1 (a=2.6 mm, $2c$=7.6 mm) at 133,000 cycles presented in Fig. 3 and Table 4 in the experiment, CP cycles with the FE models and with Mk factor formulas are evaluated. Crack depth a in the CP simulations are adjusted to BM No.1 and the fatigue cycles are counted from 133,000 cycles. Fatigue life cycles are evaluated until crack penetration.

Hot spot is defined at the radiused weld toe in the HSSs evaluation as shown for Fig. 6(b). CP result with Mk factor formulas are compared with the FEM result. It is found that result with Mk factor formulas is conservative than that of the FEM.

5.3.4 Discussion

CP phenomena of a T-shaped tubular joint with ρ=16 mm are examined employing two fatigue strength assessment methods, *i.e.*, 3D FE fracture modeling with shell-solid model and Mk factor formulas approach. Through the comparison with the fatigue test results, effectiveness of the fatigue evaluation methods is discussed.

Shell-solid modeling is effective and efficient technique to discuss fracture behaviors in a steel T-shaped tubular joint. Computation time is reduced than analysis with the solid FE model. Crack path and aspect ratio of the surface crack correlate well with the fatigue test results. Fatigue life cycles for CP are also in good correlation. And, the simulation results are slightly conservative.

A CP approach with Mk factor formulas proposed in [19,59] with UK Den HSS evaluation technique is effective to discuss the CP phenomena. Very quick simulation is developed. Although some assumptions are adopted, the similar tendency can be seen compared with the FE results and fatigue test results. In addition, the CP approach with Mk factor formulas gives conservative results than the FE results even though same material parameter C and m are employed. Linear and quadratic UK Den HSS evaluation techniques are examined. They show almost similar values but the quadratic approximation gives slightly conservative evaluation.

Yagi *et al.* [33,34] analyzed CP behaviors of T-shaped tubular joint with weld toe radii ρ=3, 6, 11 mm and the results were examined with Mk factor formulas. Through the fatigue testing and the fatigue assessments employing CP simulation results with FEM and with Mk factor approach for ρ=16 mm specimen, it is confirmed that same tendency is obtained and the simplified CP simulation give the most conservative evaluation results among three approaches when same material parameters C and m are employed.

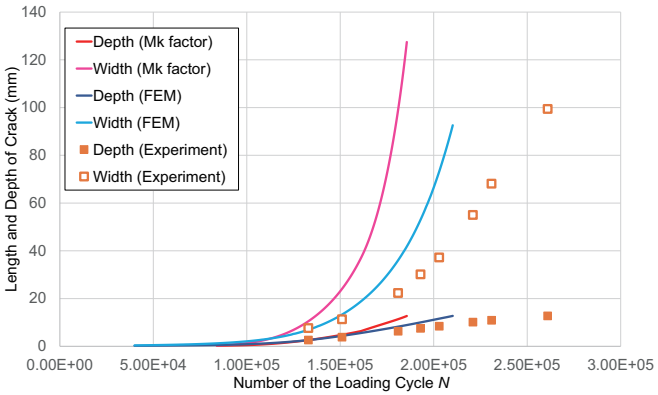

Fig. 17 Calculated CP curve

6 Conclusions

CP phenomena of a steel CHS T-joint for ρ=16 mm specimen is investigated employing an advanced CP simulation system based on a shell-solid FE model and Mk factor formulas. In Section 2, fatigue test results for the joint were shown. In Section 3, a shell-solid modeling for CP simulation is presented. In Section 4, CP simulation with Mk factor formulas are mentioned. Based on the two fatigue strength assessment methods, the experimental results are examined and discussed in Section 5. Through this paper, it is found that:

- Shell-solid modeling is effective to analyze CP behaviors for a cracked T-shaped tubular joint.
- CP simulation with Mk factor formulas is very fast. The results show good tendency compared with FE CP result. It also gives conservative results compared with FEM and experimental results in the present case.
- Fatigue life cycles are examined with two fatigue strength assessment methods. The two methods are effective to discuss the CP behaviors. CP simulation results with Mk factor formulas give conservative evaluation for the present case.

Acknowledgements The authors would like to express deep appreciation to Mr. Pavan R. (ILDP-SAP) for his valuable comments and discussions. The authors' sincere gratitude extends to Dr. Yosuke Kobayashi (TechnoStar Co., Ltd.) for supporting the software operation.

References

1. ISO 19902 (2007) Petroleum and natural gas industries – Fixed steel offshore structures
2. Yagi J, Machida S, Matoba M, Tomita Y, Soya I (1993) Thickness effect criterion for fatigue strength evaluation of welded steel structures. J Offshore Mech Arctic Eng 115:58-65
3. Hobbacher AF ed. (1996) Recommendations for fatigue strength of welded components. Cambridge: Abington Publishers
4. van Wingerde AM, Packer JA, Wardenier J (1995) Criteria for the fatigue assessment of hollow structural section connections. J Constr Steel Res 35:71-115
5. Osawa N, Yamamoto N, Fukuoka T, Sawamura J, Nagai H, Maeda S (2011) Study on the preciseness of hot spot stress of web-stiffened cruciform welded joints derived from shell finite element analyses. Mar Struct 24:207-238
6. Sumi Y (2014) Fatigue crack propagation in marine structures under seaway loading. Int J Fatig 58:218-224
7. He W, Liu J, Xie D (2014) Numerical study on fatigue crack growth at a web-stiffener of ship structural details by an objected-oriented approach in conjunction with ABAQUS. Mar Struct 35:45-69
8. Qiao W, Sun J, Xie D (2014) Development of super element to perform direct analysis on failure assessment of hull structures based on FAD. Mar Struct 39:373-394
9. Tanaka S, Kawahara T, Okada H (2014) Study on crack propagation simulation of surface crack in welded joint structure. Mar Struct 39:315-334
10. Tanaka S, Okada H, Okazawa S, Fujikubo M. Fracture mechanics analysis using the wavelet Galerkin method and extended finite element method. Int J Numer Meth Eng 93:1082-1108
11. Matsuda K, Gotoh K (2015) Numerical simulation of fatigue crack propagation under superimposed stress histories containing different frequency components with several mean stress conditions. Mar Struct 41:77-95
12. Gotoh K, Niwa T, Anai Y (2015) Numerical simulation of fatigue crack propagation under biaxial tensile loadings with phase differences. Mar Struct 42:53-70
13. Gadallah R, Osawa N, Tanaka S, Tsutsumi S (2018) Critical investigation on the influence of welding heat input and welding residual stress on stress intensity factor and fatigue crack propagation. Eng Fail Anal 89:200-221
14. Dai MJ, Tanaka S, Sadamoto S, Yu TT, Bui TQ (2020) Advanced reproducing kernel meshfree modeling of cracked curved shells for mixed-mode stress resultant intensity factors. Eng Fract Mech 233:107012
15. Maddox SJ (2002) Fatigue strength of welded structures, 2nd *ed.*. Woodhead Publishing
16. Fricke W (2003) Fatigue analysis of welded joints: state of development. Mar Struct 16:185-200
17. Department of Energy, UK, Offshore Installations (1990) Guidance on design, construction and certification, LONDON:H.M.S.O.
18. Det Norske Veritas (2011) Fatigue design of offshore steel structures, DNV-RP-C203
19. Bowness D, Lee MMK (2002) Fracture mechanics assessment of fatigue cracks in offshore tubular structures, OTO Report 2000/077. Health and Safety Executive https://www.hse.gov.uk/research/otopdf/2000/oto00077.pdf [accessed 21.3.10].
20. Lee MMK, Bowness D (2002) Estimation of stress intensity factor solutions for weld toe cracks in offshore tubular joints. Int J Fatig 24:861-875
21. Qian X, Dodds Jr. RH, Choo YS (2005) Mode mixity for circular hollow section X joints with weld toe cracks. J Offshore Mech Arctic Eng 127:269-279
22. Qian X, Dodds Jr. RH, Choo YS (2006) Mode mixity for tubular K-joints with weld toe cracks. Eng Fract Mech 73:1321-1342
23. Qian X (2013) Failure assessment diagrams for circular hollow section X- and K-joints. Int J Pres Ves Pip 104:43-56

24. Qian X, Ou Z, Swaddiwudhipong S, Marshall PW (2013) Brittle failure caused by lamellar splitting in a large-scale tubular joint with fatigue cracks. Mar Struct 34:185-204
25. Wang X, Lambert SB (2003) On the calculation of stress intensity factors for surface cracks in welded pipe-plate and tubular joints. Int J Fatig 25:89-96
26. Qiang B, Wang X (2020) Evaluating stress intensity factors for surface cracks in an orthotropic steel deck accounting for the welding residual stresses. Theor Appl Fract Mech 110:102827
27. Ahmadi H, Lotfollahi-Yaghin MA, Aminfar MH (2011) Distribution of weld toe stress concentration factors on the central brace in two-planer CHS DKT-connections of steel offshore structures. Thin-Walled Struct 49:1225-1236
28. Ahmadi H, Lotfollahi-Yaghin MA, Aminfar MH (2011) Geometrical effect on SCF distribution in uni-planer tubular DKT-joints under axial loads. J Constr Steel Res 67:1282-1291
29. Ahmadi H, Lotfollahi-Yaghin MA (2012) A probability distribution model for stress concentration factors in multi-planar tubular DKT-joints of steel offshore structures. Appl Ocean Res 34:21-32.
30. Ahmadi H, Lotfollahi-Yaghin MA (2015) Stress concentration due to in-plane bending (IPB) loads in ring-stiffened tubular KT-joints of offshore structures: Parametric study and design formulation. Appl Ocean Res 51:54-66
31. Gadallah R, Tsutsumi S, Tanaka S, Osawa N (2020) Accurate evaluation of fracture parameters for a surface-cracked tubular T-joint taking welding residual stress into account. Mar Struct 71:102733
32. Maeda K, Tanaka S, Takahashi H, Yagi K, Osawa N (2021) Mechanical evaluation for a fatigue fracture surface generated in steel T-shaped tubular joints with different weld toe radius. J Soc Naval Arch Japan 32:141-152 (in Japanese)
33. Yagi K, Tanaka S, Kawahara T, Nihei K, Okada H, Osawa N (2017) Evaluation of crack propagation behaviors in tubular T-joints. Int J Fatig 96:270-282
34. Yagi K, Osawa N, Tanaka S, Kuroda K (2018) Study on SN-based and FCP-based fatigue assessment techniques for T-shaped tubular welded joint. J Soc Naval Arch Japan 28:13-26 (in Japanese)
35. TechnoStar Co.,Ltd. (2016) TSV-Crack V6.6 Manual Rev1
36. Okada H, Kawai H, Araki K (2008) A virtual crack closure-integral method (VCCM) to compute the energy release rates and stress intensity factors based on quadratic tetrahedral finite elements. Eng Fract Mech 75:4466-4485
37. Department of Energy (1984) Background to new fatigue design guidance for steel welded joints in offshore structures. H.M.S.O.
38. Newman Jr. JC, Raju IS (1981) An empirical stress-intensity factor equation for the surface crack. Eng Fract Mech 15:185-192
39. Hirai I, Wang BP, Pilkey WD (1984) An efficient zooming method for finite element analysis. Int J Numer Meth Eng 20:1671-1683
40. Sun CT, Mao KM (1988) A global-local finite element method suitable for parallel computations. Comput Struct 29:309-315
41. Whitcomb JD (1991) Iterative global/local finite element analysis. Comput Struct 40:1027-1031
42. Nakasumi S, Suzuki K, Fujii D, Ohtsubo H (2003) Mixed analysis of shell and solid elements using the overlaying mesh method. J Mar Sci Tech 7:180-188
43. Nakasumi S, Suzuki K, Ohtsubo H (2008) Crack growth analysis using mesh superposition technique and X-FEM. Int J Numer Meth Eng 75:291-304
44. Tanaka S, Okada H, Watanabe Y, Wakatsuki T (2006) Applications of s-FEM to the problems of composite materials with initial strain-like terms. Int J Multiscale Comput Eng 4:411-428
45. Ooya T, Tanaka S, Okada H (2009) On the linear dependencies of interpolation functions in s-version finite element method. J Comput Sci Tech 3:124-135
46. Osawa N, Hashimoto K, Sawamura J, Nakai T, Suzuki S (2007) Study on shell-solid coupling FE analysis for fatigue assessment of ship structure. Mar Struct 20:143-163
47. Tanaka S, Okazawa S, Okada H, Xi Y, Ohtsuki Y (2013) Analysis of three-dimensional surface crack in welded joint structure using shell-solid mixed method. Int J Offshore Polar Eng 23:224-231
48. Cofer WF, Will KM (1991) A three-dimensional, shell-solid transition element for general nonlinear analysis. Comput Struct 38:449-462
49. Gmür TC, Schorderet AM (1993) A set of three-dimensional solid to shell transition elements for structural dynamics. Comput Struct 46:583-591
50. McCune RW, Armstrong CG, Robinson DJ (2000) Mixed-dimensional coupling in finite element models. Int J Numer Meth Eng 49:725-750
51. Shim KW, Monaghan DJ, Armstrong CG (2002) Mixed dimensional coupling in finite element stress analysis. Eng Comput 18:241-252
52. Marc 2010, User's Guide.
53. Tanaka S, Sujiatanti SH, Setoyama Y, Yu J, Yanagihara D, Pei Z (2019) Buckling and collapse analysis of a cracked panel under a sequence of tensile to compressive load employing a shell-solid mixed finite element modeling. Eng Fail Anal 104:987-1001
54. Maddox SJ (1975) An analysis of fatigue cracks in fillet welded joints. Int J Fract 11:221-243
55. Niu X, Glinka G (1987) The weld profile effect on stress intensity factors in weldments. Int J Fract 35:3-20
56. Hobbacher A (1992) Stress intensity factors of plates under tensile load with welded-on flat side gussets. Eng Fract Mech 41:897-905
57. Hobbacher A (1993) Stress intensity factors of welded joints. Eng Fract Mech 46:173-182
58. Fu B, Haswell JV, Bettess P (1993) Weld magnification factors for semi-elliptical surface cracks in fillet welded T-butt joint models. Int J Fract 63:155-171
59. Bowness D, Lee MMK (2000) Prediction of weld toe magnification factors for semi-elliptical cracks in T-butt joints. Int J Fatig 22:369-387
60. Bowness D, Lee MMK (2000) Weld toe magnification factors for semi-elliptical cracks in T-butt joints - comparison with existing solutions. Int J Fatig 22:389-396.
61. Newman Jr. JC, Raju IS (1981) Stress-Intensity factor equations for cracks in three-dimensional finite bodies. NASA Technical Memorandum 83200 https://ntrs.nasa.gov/api/citations/19810023035 /downloads/19810023035.pdf [accessed 21.3.10].
62. MSC.Nastran 2010. User's Guide.
63. Fatigue design recommendation for steel structures (2012) JSSC
64. Dell'Erba DN, Aliabadi MH (2000) Three-dimensional thermo-mechanical fatigue crack growth using BEM. Int J Fatig 22:261-273
65. Erdogan F, Sih GC (1963) On the crack extension in plates under plane loading and transverse shear. J Basic Eng Trans ASME 85:519-527.